Molecular Dynamics Study on Mechanical Properties of Calcium–Silicate–Hydrate Considering Model and Parameter Effects

Xuefeng Wang, Meiyi Li, Congcong Lv, Yunfeng Han, and Hang Yin

Abstract The micro and nano scale composition in concrete is one of the essential topics at the moment. At nanoscale, calcium–silicate–hydrate (C–S–H) gel is the main material phase that determines the mechanical properties in cement hydration. In the past decade, a lot of research work has been developed based on the molecular structure of C–S–H gels. Since its structure is difficult to be uniquely determined by experimental methods, the diversity of models and parameters may lead to differences in calculation results when characterizing C–S–H properties. Therefore, this paper mainly focuses on the comparative study of the common model structures and force field parameters in C–S–H molecular dynamics simulations, and specifically discusses the effects of mechanical properties with Hamid and Merlino tobermorite structures, silica-oxygen tetrahedral distribution, OH groups, water models and force fields. The research results show that the differences in models and parameters have indistinctive influence on the value of the elastic modulus, and the anisotropy of the molecular structure is generally consistent. However, the two tobermorite structures, the uniform distribution of silica groups, and the setting of the force field have obvious differences in plastic deformation and fracture behaviors. When studying large deformation and creep, it is necessary to choose the model structure and parameters carefully. The elastic modulus and mean square displacement calculated based on different water models have consistent regularity. The choice of water model has a significant impact on viscosity and interfacial adhesion, which needs to be considered when studying water diffusivity and drying shrinkage. The research results provide detailed guidance and suggestions for the model and parameter selection of further studies in C–S–H molecular dynamics simulation.

X. Wang · M. Li · Y. Han · H. Yin (✉)
College of Water Conservancy and Civil Engineering, Shandong Agricultural University, Tai'an 271018, China
e-mail: yinh@sdau.edu.cn

X. Wang · C. Lv · H. Yin
Hubei Key Laboratory of Construction and Management in Hydropower Engineering, China Three Gorges University, Yichang 443002, China

S. Li (ed.), *Computational and Experimental Simulations in Engineering*, Mechanisms and Machine Science 146, https://doi.org/10.1007/978-3-031-44947-5_68

Keywords Concrete · Calcium–silicate–hydrate · Mechanical property · Molecular dynamics

1 Introduction

The study of micro- and nano-scale composition in concrete is one of the essential topics at the moment [1]. Calcium–silicate–hydrate (C–S–H) gel is the main material phase in cement hydration products that determines many properties at nano-scale. Due to the complexity of hydration process, the diversity of the morphology and composition in C–S–H gels leaves great challenges of characterization methods. In order to study the intrinsic properties and mechanisms of C–S–H, a series of atomic structure models have been developed based on the evolution of theoretical models [2]. It can be regarded as a bottom-up way of studying C–S–H gels. Molecular dynamics (MD) simulations can accurately describe chemical processes (e.g., chemical bond formation and breaking) and physical state changes in atomic systems, which drives much attention in nanoscale properties and mechanisms such as structure, mechanical properties, and interfacial interactions of atomistic C–S–H in the past decade [1, 3]. The C–S–H calculation model is not unique with certain molecular formula, which is usually obtained based on several random modification and adjustment of tobermorite crystals.

There are two general types of 1.1 nm tobermorite structures, namely the Hamid structure [4] and the Merlino structure [5]. Both of the structures have been carried out in the current MD simulations of C–S–H [6–10]. For example, Hou et al. [11] studied the tensile mechanical properties of Hamid C–S–H models with different Ca/Si ratio. There is an agreement of decreasing trend of tensile strength and elastic modulus with the increasing Ca/Si ratio. It is due to the average chain length of silicates becomes shorter at higher ratios, and more water enters the defect region which weakening the stability of C–S–H gels [12]. Sarkar et al. [9] studied the molecular deformation response of 1.1 nm tobermorite under uniaxial/triaxial loading using Merlino structure using empirical force field and reaction force field. Furthermore, the quantitative information on the fractions of Si present in silicate tetrahedra with different connectivity is generated from ^{29}Si nuclear magnetic resonance (NMR) [13, 14], which provides a basis for theoretical modeling. The obtained Q_n distribution is prefer to act as several ranges rather than specific values. There is no relevant detailed description of the exact positions of the silicate tetrahedra with different connectivity. Many researches follow up Pellenq's modeling process [15], while some of the studies further considered the process of water molecules dissociate to generate OH groups and binds to Si and Ca ions [16, 17].

Except the modeling issues, the choice of force field can also affect the simulation results of C–S–H. The force fields commonly used for C–S–H gels are ClayFF [18], CSHFF [19], and ReaxFF [20], and each of them has different applications and advantages in MD simulations of cementitious materials. Some researchers have used these force fields to simulate the molecular deformation of 1.1 nm tobermorite under

different loading conditions, which lead to a wide range of variations in the results [21–23]. The mechanical properties of cementitious materials can be significantly influenced by the changes in water content [24]. The choice of water models is also the part of force field. The first water model was proposed by Bernal and Fowler and benchmarked against measured vibrational energy levels of water [25]. Since then several different classical water models have been proposed [26]. The water model is less frequently discussed in MD simulations of C–S–H gels.

In general, several MD studies have focused on the mechanical properties of C–S–H gels, but the effects of C–S–H models and force field parameters on simulation results have not been systematically discussed.

Therefore, this paper specifically applied a series of MD simulations to study the effects of mechanical properties with calculation settings, including Hamid and Merlino tobermorite structures, silica-oxygen tetrahedral distribution, OH groups, water models and force fields.

2 Simulation Methods

2.1 C–S–H Cell Model

Two different types of molecular structure has been used by researchers to represent the crystal structure of tobermorites: e.g. Merlino structure [5] and the Hamid structure [4]. The Hamid structure calcium silicate layer exists alone (Fig. 1a) and the upper and lower layers are oriented in opposite directions (circle by solid-line in Fig. 1a), while the Merlino structure has Si–O–Si bonds between the intermediate layers (Fig. 1b) and the upper and lower layers are oriented in the same direction (circle by solid-line in Fig. 1b). Then, on the basis of these two structures, the C–S–H molecular model was established by referring to the Pellenq [15] method. Firstly, A part of SiO_2 (neutral) molecules are then randomly removed for satisfying the distributions of Q species obtained from NMR testing [27]. Since the effect of oxhydryl (OH group) on the mechanical property of C–S–H is small [15, 28], it was not considered in the present work without special remarks. Secondly, Grand Canonical Monte Carlo simulation of the water adsorption is operated at 300 K to saturate the structure and close to the result obtained by the small angle neutron scattering (SANS) test [17]. Finally, a further 1000 ps relaxation at the NPT (N: number of atoms; P: pressure; T: temperature of system) ensemble (isothermal isobaric ensemble) is conducted to achieve the structures of C–S–H gel in equilibrium states.

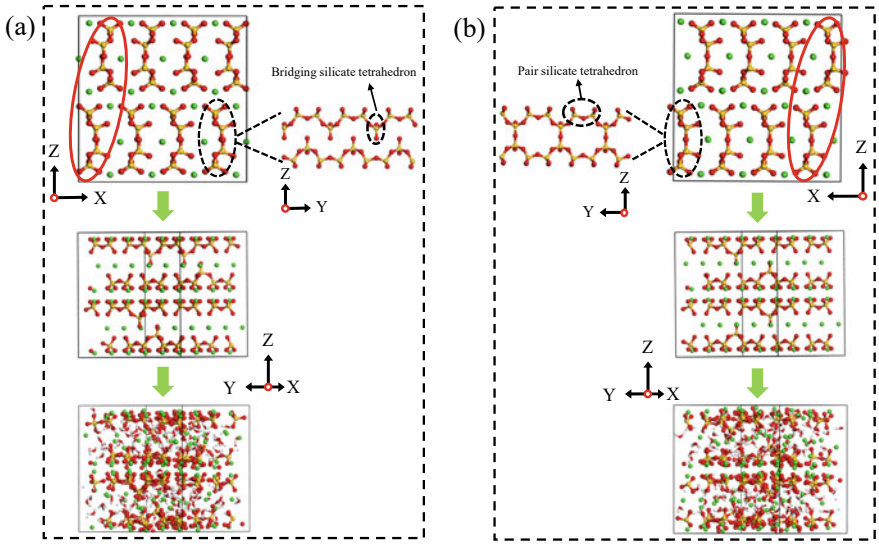

Fig. 1 Molecular model of 1.1 nm tobermorite. **a** Hamid structure; **b** Merlino structure

2.2 Modeling and Simulation Details

The MD simulations in this study were performed on the open-source code 'Large-scale Atomic/Molecular Massively parallel Simulator' (LAMMPS) developed by Plimpton [29]. The simulation cell of each C–S–H, after MD equilibration, is subjected to three uniaxial tension/compression pairs and three pure shear pairs. For example, when testing the properties along the z-direction, we first created a supercell containing 2(x) × 2(y) × 4(z) modified cells for uniaxial tests. The supercell is then relaxed under the isothermal isobaric (NPT) ensemble with T = 300 K and P = 0, and the equilibrium configuration is achieved after 10 ps of relaxation. Finally, the C–S–H structure is elongated in the z-direction with strain rate of 0.008/ps under the NPT ensemble with Px = Py = 0. Pz indicates the internal stress σ_{zz} along the z-direction. The time integration of the motion equation was performed by using the Verlet leapfrog algorithm with a time step of 0.1 fs. The electrostatic Coulombic interactions were evaluated by the Edward summation method with a cutoff of 1.0 nm.

The mechanical properties of C–S–H gel exhibits anisotropic due to their molecular structure at nanoscale, while the cement behaves isotropic at macroscale [30, 31]. To quantify the anisotropy at the nanoscale, we use the Reuss Voigt Hill (R-V-H) average method [32] to predict the indentation modulus $M_{\text{R-V-H}}$ [28] and Poisson's ratio μ of C–S–H, i.e.,

$$M_{R-V-H} = 4G\frac{3K+G}{3K+4G}, \tag{1}$$

$$\mu_{R-V-H} = \frac{1}{2}\left(1 - \frac{3G}{3K+G}\right), \tag{2}$$

where K and G are the mean values of bulk and shear moduli calculated by Voigt method [33] and Reuss method [34], respectively (Hill method).

In the paper, unless noted, the model uses the Hamid structure, the force potential uses ClayFF.

3 Results and Discussion

3.1 Comparison of the Tobermorite of Hamid and Merlino

In this section, we discuss the performance differences between the Merlino and the Hamid structure. When constructing the C–S–H molecular model, the positions of the two structural defects in silicate chains and various components were set to be the same in order to exclude external factors as far as possible.

Different stress–strain curves (Fig. 2a) of tensile loading in x, y and z direction indicated heterogeneous nature of C–S–H layered structure. The tensile strengths of Hamid structure in x, y and z directions ($H_x = 3.15$ GPa, $H_y = 3.19$ GPa, $H_z = 1.62$ GPa) are smaller than those of Merlino structure ($H_x = 3.37$ GPa, $H_y = 3.42$ GPa, $H_z = 1.88$ GPa). The Hamid structure exhibits better ductility with larger fracture strains in the x, y, and z directions than the Merlino structure. The stress in the x-direction of the Hamid structure does not decrease to 0 after reaching to maximum value. The yield stage shows good plasticity. As shown in Fig. 2b, there are only the low-density regions in the black dashed circles instead of fracture when the strain reaches 0.8.

The $M_{R\text{-}V\text{-}H}$ of Hamid model is 50.94 GPa, while the $M_{R\text{-}V\text{-}H}$ of Merlino model is 48.37 GPa (Fig. 3a). The percentage deviation of $M_{R\text{-}V\text{-}H}$ is 5.0%. We also compared the modulus of elasticity in uniaxial tension, which is evaluated at the initial stage of the stress–strain curve, such as the line segment in the dashed circle in Fig. 2a. The deviations of the elastic modulus x_T, y_T, and z_T in the three directions are 1.7%, 3.0%, and 2.3%, respectively, with a slightly larger deviation in the y direction. This is due to the y-direction is the main direction of the silicon chain, and the Si–O bond is the key to determine the mechanical properties of C–S–H. The deviation in the arrangement of the silicon chain is also the main difference between the two structures (Fig. 1) The $M_{R\text{-}V\text{-}H}$ values measured for both structures are smaller than x_T and y_T and larger than z_T, while the Poisson's ratio exhibits: $\mu_{R\text{-}V\text{-}H} > \mu_x > \mu_y > \mu_z$, with μ_x deviating more. The Ca–O bond is defined when the calcium-oxygen distance is shorter than 0.30 nm according to the criterion proposed by Hou et al. [8]. We counted the relationship between the number distribution of Ca–O bonds in single cell C–S–H gels (Fig. 4), and it is obvious that the strength of the Ca–O bond is greater in the Merlino structure than in the Hamid structure. Therefore, the

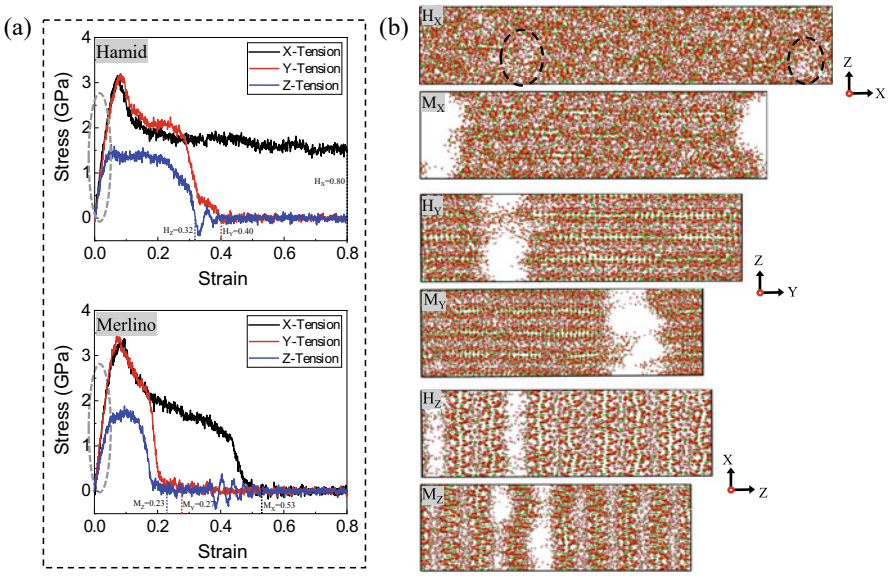

Fig. 2 The stretching process of C–S–H supercells with Hamid and Merlino structures stretched along three different directions. **a** The stress–strain curves; **b** fracture of the C–S–H layers

deformation of the Merlino structure is suppressed, resulting in a smaller Poisson's ratio.

To verify the accuracy of the above results, they were compared with other simulations as well as the values provided by experimental studies. The $M_{R\text{-}V\text{-}H}$ values as well as the Poisson's ratio $\mu_{R\text{-}V\text{-}H}$ for both structures were greater than the experimental values [35–37]. It is probably due to the C–S–H models of MD simulations do not take into account the stacking density and pore space. The elastic moduli fitted by uniaxial tensile simulations are closer to the results of other simulations

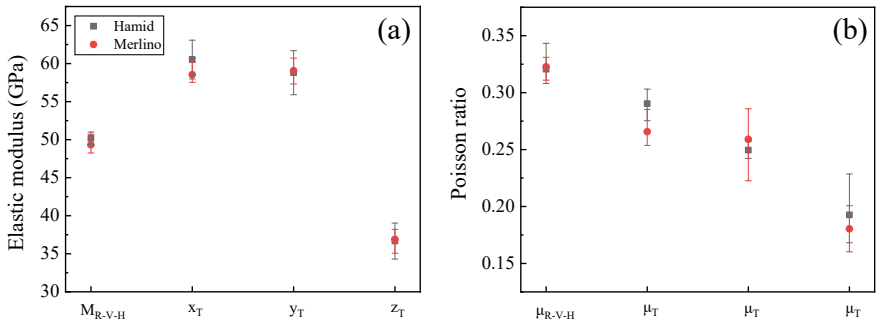

Fig. 3 Mechanical properties of Hamid and Merlino structures. **a** Elastic modulus; **b** Poisson's ratio

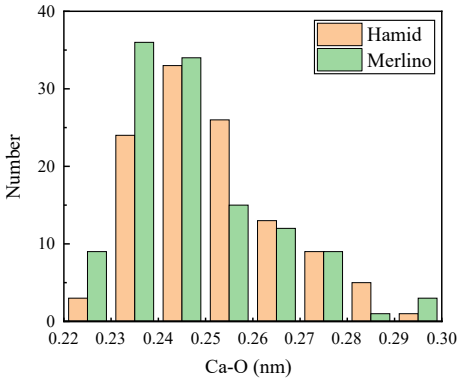

Fig. 4 The histograms of the Ca–O bond distances of Hamid and Merlino structures

[12, 21, 38, 39], and μ_x, μ_y, and μ_z are slightly smaller than the results of other simulations [40, 41]. Based on the ranges provided, the estimates obtained from the MD simulations can be considered fully acceptable and within a reasonable range.

Radial distribution function is an effective way to characterise the structure information of crystal and amorphous phases, which is given as the following formula, i.e.,

$$g(r) = \frac{dN}{4\pi r^2 \rho}, \tag{3}$$

where r is the system density, dN represents the number of atoms, and the distance between the atoms and the centre is $r \rightarrow r + dr$. Figure 5 shows three different RDFs. It can be seen that the peak RDF curves of Cw-Ow for both structures are located at ~ 2.5 Å, which is very close to the theoretical (2.37 Å) and experimental (2.41 Å) values reported by Tongraar et al. [42] and Soyer-Uzun et al. [43]. For the Si–O bond, the peak of the Hamid structure is located at ~ 1.7 Å, while the peak of the Merlino structure is located at ~ 1.5 Å, which is similar to the results of Merlino [44] and Soyer-Uzun [43]. The Ow-H bond has two peaks at ~ 1.7 and ~ 3.1 Å, which are similar to the results measured by MD simulations of Hou et al. [8]. The RDF peaks of the two structures are very close to each other. The results in Fig. 5 show that there is little difference in accuracy between the two structures in terms of bond length.

3.2 Effect of Silica-Oxygen Tetrahedron Distribution

The distribution of silica-oxygen tetrahedron is an important parameter affecting the mechanical properties of C–S–H gels [15, 16]. However, inhomogeneous distribution of silica chains (Fig. 6) and imprecise composition (Q_n) according to NMR results [27] can affect the modeling process, which brings an impact on the study of the mechanical properties of C–S–H gels.

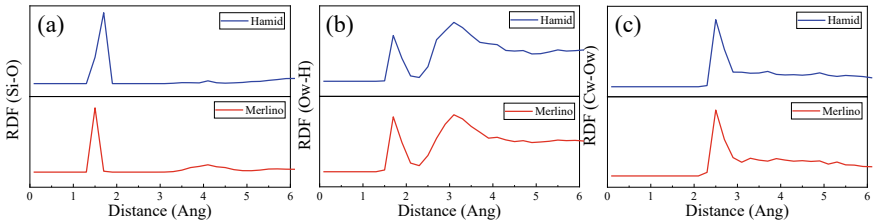

Fig. 5 The RDF comparison of Hamid and Merlino structures. **a** Si–O pairs; **b** Ow–H pairs; **c** Cw–Ow pairs

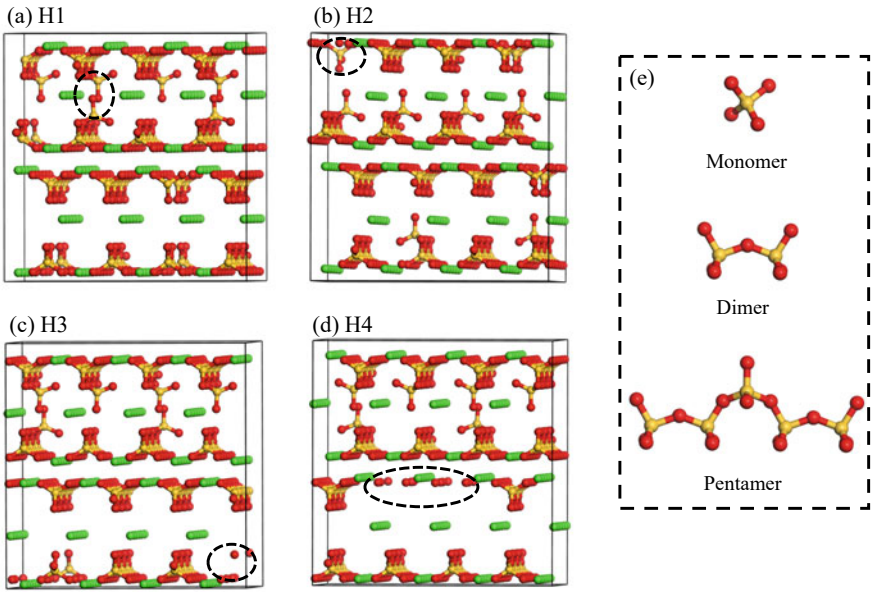

Fig. 6 Initial dry C–S–H structure of different silicon chain distributions

In this paper, we only construct the C–S–H model by breaking the bridging silica to satisfy the condition. Therefore, the prominent positions (circle by dash-line in Fig. 6a) are the locations of the pentamers. In Fig. 6a, the pentamers are all on one side, in Fig. 6b there is only one silica-oxygen tetrahedron at the dotted circle, in Fig. 6c, the pentamers are all on one side and all silica-oxygen tetrahedra with one chain are deleted, and in Fig. 6d, the pentamers are all on one side and all silica-oxygen tetrahedra with two chains are deleted. The Q_n distributions of the models in Fig. 6 are identical.

Compared with the stress–strain curves with uniform distribution of silicon chains (Fig. 7a), the rest three groups show different degrees of reduction in fracture strain and changes in tensile strength. It is mainly due to the non-uniform distribution of silicon chains, which leads to different degrees of defects and consequently changes

in mechanical properties. This may explain the discrepancies in the results of previous studies [7, 21–23, 38, 45]. In Fig. 8a, it can be seen that the silicon chain distribution has an effect on the elastic modulus of C–S–H. Among them, the y-axis direction has the most obvious effect. It is also related to the direction of silicon chain and the Si–O bond in C–S–H, resulting in a slightly larger deviation of the elastic modulus in the y-direction. Therefore, in the process of modeling, it is better to avoid the appearance of the gathering of defects and ensure the uniform distribution of monomers, dimers and pentamers in the upper and lower layers.

In addition to the degree of uniformity of silica chain distribution on C–S–H, Q_n distribution is also an important parameter affecting the mechanical properties of C–S–H gels. Four groups of different Q_n distribution from NMR test [27] are given in Table 1. Among them, the positions of silica-oxygen tetrahedra deletion are basically the same. It can be seen from Fig. 8b that a small change in Q_n distribution does not have a large effect on the elastic modulus. Therefore, the Q_n distribution is not fixed and changes in a small range do not cause a large impact on the structural properties.

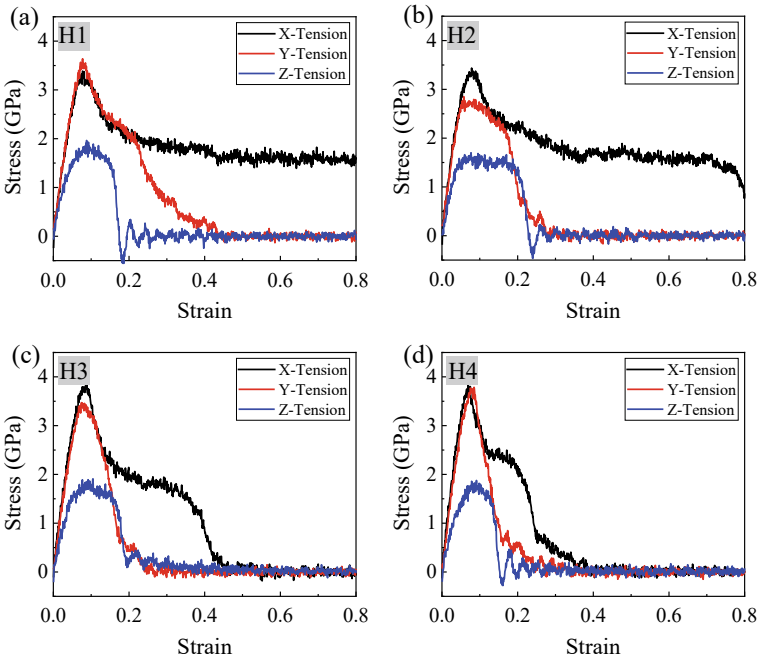

Fig. 7 Stress–strain curves of different silicon chain distributions

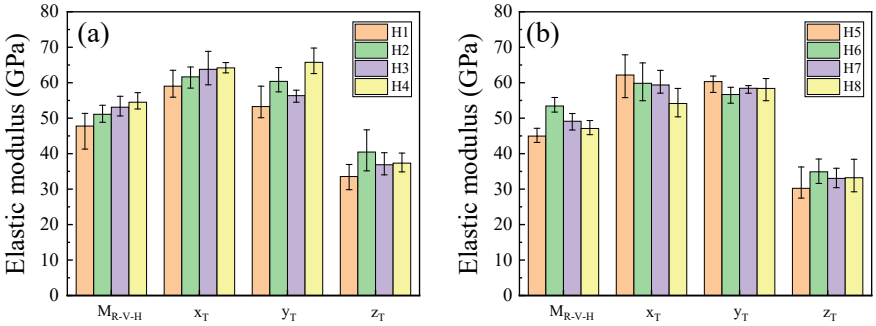

Fig. 8 Elastic modulus comparison. **a** Uniformity of silicon chain distribution (H1, H2, H3, H4); (b) Q_n distribution (H5, H6, H7, H8)

Table 1 Q_n distribution of four groups according to NMR test

Model	Monomer (Q_0) (%)	Dimer (Q_1) (%)	Pentamer (Q_2) (%)
H5	8.23	70.59	21.18
H6	12.94	65.88	21.18
H7	9.41	65.88	24.71
H8	7.06	68.24	24.71

3.3 Effect of OH Group

In this section, we consider the effect of OH groups when compared with original C–S–H model. We use ReaxFF [46] to perform semi-classical MD simulations that allow the reaction of inserted water molecules with interlayer calcium and silica groups. In this stage, some interlayer water molecules dissociate into hydroxyl groups and protons. The sample is equilibrated within ReaxFF for a limited trajectory duration. In the process of distinguishing between different types of oxygen, hydrogen and calcium atoms, a full topological analysis is performed to identify the local environment of the species. This facilitates the transition from the use of ReaxFF to ClayFF. Finally, a final equilibration of the model is performed using ClayFF. In addition, the water model is normally regarded as rigid molecule, while ClayFF treated water molecule as flexible SPC model. We also make a comparison in this section.

As shown in Fig. 9a, comparing the initial model with the model considering OH, there is no uniform pattern in the elastic modulus in the x and y directions, and the $M_{R\text{-}V\text{-}H}$ values are similar, which indicates that the OH group has a low effect on the elastic modulus in general. In the z-direction, the elastic modulus decreases in both directions when OH group is considered. The oxygen atoms on the silicon chains of the intermediate layers combine with hydrogen atoms to form hydroxyl groups, which are mainly concentrated in the interlayer direction, leading to an increase in the interlayer distance (Fig. 9c) and a decrease in the Coulombic gravitational force

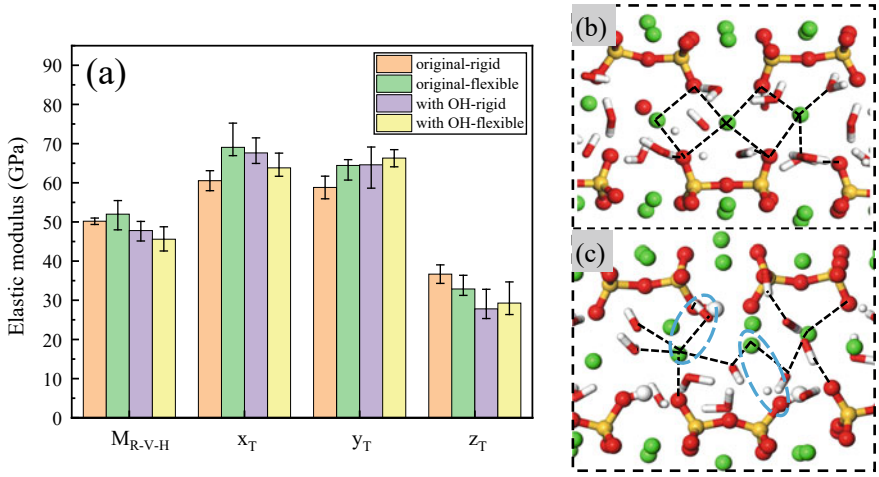

Fig. 9 **a** Elastic modulus comparison of each models; Schematic diagram of bonding changes in **b** C–S–H original model and **c** C–S–H with OH group

between adjacent calcium silicate layers [8]. At the same time, due to the increase of interlayer distance, more H–O bonds are needed to link the calcium-silica plates, and the originally formed Ca–O bonds may disappear due to the increase of interlayer distance (Fig. 9c), which in turn leads to the decrease of mechanical properties.

When compared with the rigid and flexible water model, its effect on elastic modulus in the original C–S–H model is significantly larger than that of considering the OH group. It is probably due to the existence of OH groups implying that the number of water molecules have already reduced. When OH groups are involved in the C–S–H gel, whether the water molecules are set to be flexible or not has less effect on the elastic modulus.

3.4 Comparison of Computational Water Models

In this section, we further discuss the effect of four commonly used water models, i.e. SPC [47], SPC/E [48], TIP3P [49], and TIP4P [50]. The interaction potential parameters are shown in Table 2. For the comparison of these water models in the C–S–H structure, the number and position of water molecules in the equilibrium structure are initially the same and are achieved by replacing these water molecules at the same oxygen atom coordinate positions as in the SPC model.

From Fig. 10, it can be seen that the elastic modulus calculated using the four water models is very close to each other and the differences can be negligible. The stress–strain curves through the whole process of uniaxial tensile loading in z-direction can be found that the SPC/E and TIP3P models have the smallest differences in the

Table 2 Interaction potential parameters of the five classical molecular water models considered

Parameters						
Model	σ (nm)	ε (kcal/mol)	b (nm)	θ (°)	q_o (e)	q_H (e)
SPC	0.31660	0.1554	0.1	109.47	− 0.8200	+ 0.4100
SPC/E	0.31660	0.1554	0.1	109.47	− 0.8476	+ 0.4238
TIP3P	0.31880	0.1020	0.09572	104.52	− 0.8340	+ 0.4170
TIP4P	0.31644	0.16275	0.09572	104.52	− 1.0484	+ 0.5242

Parameters σ and ε are nonbonding interaction parameters, respectively; b and θ are the equilibrium values of bond length and angle; q_o and q_H correspond to the charge on the hydrogen atom and oxygen atom

calculated results. The critical stress obtained by the SPC model is lower and the fracture strain is the largest. The critical stress of the TIP4P model is the largest.

To further understand the working mechanism of different water models on the creep behavior of C–S–H, two factors that influence the creep deformation were investigated: one is the viscosity of the interlayer component (water molecules) [51–53] and the other is the interfacial adhesion between the calcium silicate layers and the interlayer component [52, 54–57]. Viscosity is the material property that can be viewed as the resistance offered to change the position of molecules due to the existence of a potential barrier around the molecules in the liquid [58]. In order to expose the viscosity change of different water molecules, the atom mobility of the water molecule is described by calculating the mean square displacement (MSD) using the following equation [59], i.e.,

$$MSD(t) = \left\langle |r(t) - r(0)|^2 \right\rangle = \frac{1}{N} \sum_{n=1}^{N} |r_n(t) - r_n(0)|^2 \tag{4}$$

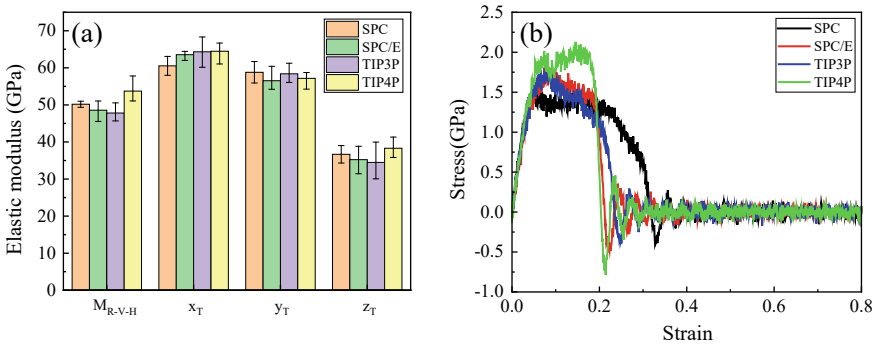

Fig. 10 Elastic modulus (**a**) and stress strain curves in z direction (**b**) of four water models in C–S–H

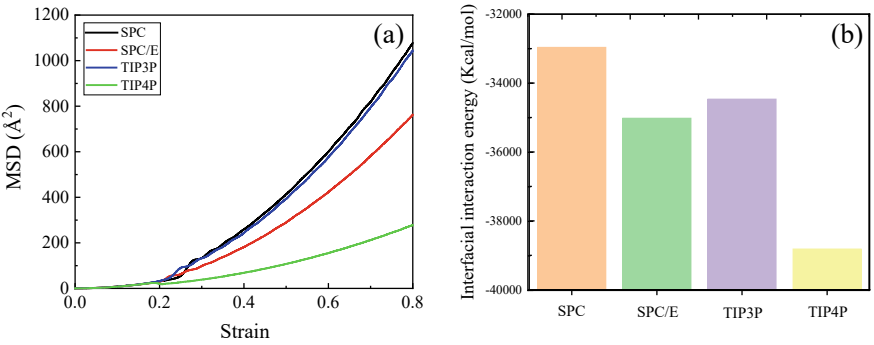

Fig. 11 **a** The MSD of various interlayer lubricator of the equilibrated C–S–H; **b** the variations of the interfacial interaction energy between calcium silicate layers and the lubricator of the equilibrated C–S–H

where N is the number of atoms to be averaged, $r_n(t)$ is the position of each atom in determined time t, $r_n(0)$ is the reference position of each atom. Figure 11a shows the mean square displacement (MSD) under the action of four water models. The mean square displacement of the SPC water model approximates the results such as Hou et al. [38], which verifies the accuracy of the results. The migration rates of the four water models are: SPC > TIP3P > SPC/E > TIP4P. SPC model has the fastest atomic migration rate, indicating the lowest viscosity and the best lubrication effect [60].

To reveal the effect of different water on the interfacial adhesion between calcium silicate layers and the interlayer component, the interfacial interaction energy, a valuable parameter to identify the interfacial adhesion, was calculated using the following equation [61], i.e.,

$$E_{\text{Inter}} = E_{\text{Total}} - E_{\text{Layer}} - E_{\text{Lub}}, \tag{5}$$

where E_{Inter} is the total potential energy of the C–S–H system, E_{Layer} is the potential energy of the calcium silicate layer, and E_{Lub} is the potential energy of the interlayer components. Figure 11b shows the interfacial interactions under the action of four water models. The magnitude of the interfacial interaction energy is in the order of SPC > TIP3P > SPC/E > TIP4P, indicating that the interfacial adhesion between the calcium silicate layer and the SPC is the weakest. The weaker interfacial adhesion also facilitates the lubrication effect [53].

3.5 Comparison of Force Potentials

The selection of the force potential is essential to study the C–S–H properties. In this section, we discuss the effect of three force fields, ClayFF [18], CSHFF [19] and ReaxFF [20], on the mechanical properties of C–S–H gels. The models required

for the comparison of the different force potentials are obtained by relaxation of the model after adsorption saturation of the ClayFF force potential.

Figure 12 shows the various moduli and stress–strain curves obtained by calculation for different force properties. As can be seen from the figure, the $M_{R\text{-}V\text{-}H}$ of CSHFF is much larger than the other two force properties. The tensile moduli x_T and z_T fitted through the initial stage also exhibit CSHFF greater than the other two force properties, and y_T exhibits a trend of ReaxFF greater than CSHFF greater than ClayFF. From the stress–strain curves, it can be seen that ClayFF has the smallest tensile strength in three directions, and CSHFF and ReaxFF are close. The stresses in the x-direction of all three force properties do not drop to zero at the late stage of damage.

The computational resources is another parameter to be considered. The tests were made with a C–S–H model with dimensions of approximately 2.23 × 2.22 × 2.28 nm and an atomic number of 998. The simulations were done in the server, using i7-8700 K cores at 3.70 GHz and 12 cores. We can simulate per day nearly 6.223 ns with ClayFF, 6.410 ns with CSHFF, and 0.135 ns with ReaxFF. The computational efficiency of ClayFF and CSHFF is close and higher.

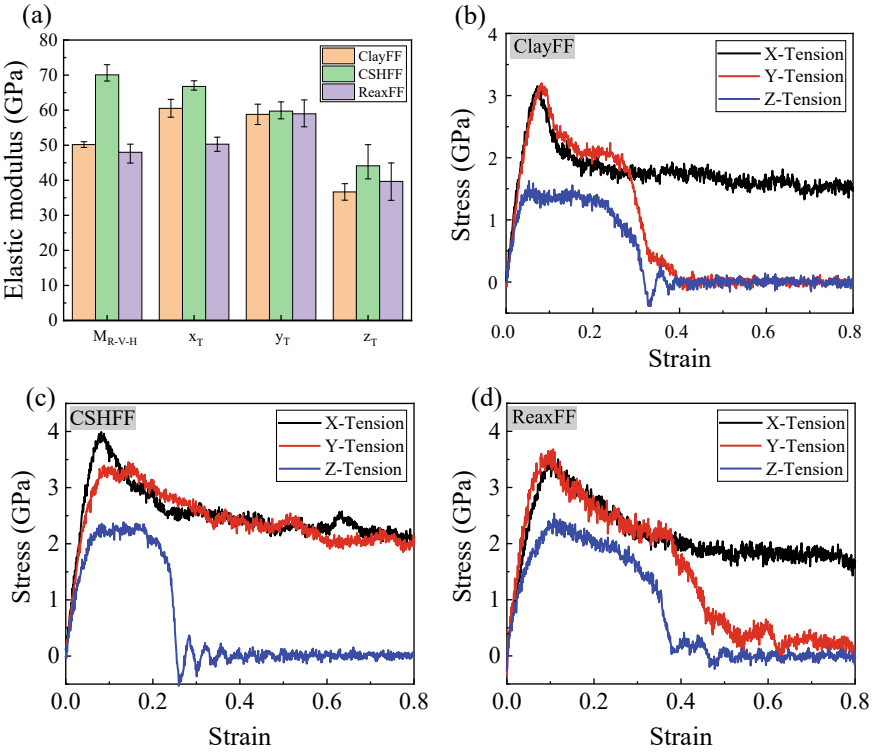

Fig. 12 Modulus comparison and stress–strain curves for three force fields

In addition to ClayFF, CSHFF, and ReaxFF, there are many force fields developed for cementitious materials, all of which have their own characteristics and application areas. Therefore, in practice, the selection should be made according to the purpose of the simulation test, etc. In the future, the research of machine learning potentials (MLPs) [62] can also be increased, and the calculation results will be faster and more accurate.

4 Conclusions

In this study, the effect of different components of the C–S–H structure on the properties was investigated by MD simulations. The differences between the Hamid and Merlino structures, the silicone tetrahedral distribution, OH groups, water molecules, and the effect of force fields were considered. In most cases, the values of elastic modulus obtained from the experimentally and theoretically developed C–S–H model and force field are close, and the z-direction is significantly smaller than the x and y-directions. When simulating amorphous C–S–H gels on larger sizes, computational efficiency can be prioritized in the model and force field selection. In contrast, the selection of relevant parameters needs to be discussed in depth when analyzing deformation and damage behavior at the molecular scale. Some detailed conclusions can be drawn as follows.

First, the elastic moduli of the Hamid and Merlino structures differ significantly only in the y direction, which mainly originates from the difference in the arrangement of the silicon chains.

Second, the degree of homogeneity of the silicon chain distribution has a large influence on the calculated elastic modulus, deformation and damage behavior. The value of Q_n obtained by NMR varies within a certain range and has a small effect on the results of mechanical property calculations.

Third, OH groups can increase the layer spacing and reduce the z-directional elastic modulus. When OH groups are not considered, the effect of rigid and flexible SPC water models on the elastic modulus is large, while the effect of different classes of water models on the elastic modulus can be neglected. The magnitudes of mobility as well as interfacial interaction energy are in the following order: SPC > TIP3P > SPC/E > TIP4P. The larger mobility as well as interfacial interaction energy indicates a weaker viscosity as well as interfacial adhesion, which is beneficial to the lubrication effect between C–S–H layers.

Finally, the $M_{R\text{-}V\text{-}H}$ modulus of CSHFF is much larger than that of ClayFF and ReaxFF, and x_T is similarly larger than that of ClayFF and ReaxFF, with a smaller difference between y_T and z_T. The operational efficiency of ReaxFF is much smaller than that of ClayFF and CSHFF.

Acknowledgements The authors acknowledge financial support from Shandong Provincial Natural Science Foundation, China (Grant No.: ZR2021MA067) and the Scientific Research Foundation of Shandong Agricultural University (Grant No.: 130/72130). The authors are greatly

thankful to the calculation support of High Performance Computing Center at Shandong Agricultural University.

References

1. Xu, J., Chen, X., Yang, G., Niu, X., Chang, F., Lacidogna, G.: Review of research on micromechanical properties of cement-based materials based on molecular dynamics simulation. Constr. Build. Mater. **312**, 125389 (2021)
2. Duque-Redondo, E., Bonnaud, P.A., Manzano, H.: A comprehensive review of C–S–H empirical and computational models, their applications, and practical aspects. Cem. Concr. Res. 156 (2022)
3. Abdolhosseini Qomi, M.J., Brochard, L., Honorio, T., Maruyama, I., Vandamme, M.: Advances in atomistic modeling and understanding of drying shrinkage in cementitious materials. Cem. Concr. Res. **148**, 106536 (2021)
4. Hamid, S.A.: The crystal structure of the 11 Å natural tobermorite $Ca_{2.25}[Si_3O_{7.5}(OH)_{1.5}] \cdot 1H_2O$. Z. Kristallogr. Cryst. Mater. **154**, 189–198 (1981)
5. Merlino, S., Bonaccorsi, E., Armbruster, T.: The real structure of tobermorite 11 Å: normal and anomalous forms, OD character and polytypic modifications. Eur. J. Mineral. **13**, 577–590 (2001)
6. Lin, W., Zhang, C., Fu, J., Xin, H.: Dynamic mechanical behaviors of calcium silicate hydrate under shock compression loading using molecular dynamics simulation. J. Non-Cryst. Solids Cryst. Solids **500**, 482–486 (2018)
7. Sadat, M.R., Muralidharan, K., Zhang, L.: Reactive molecular dynamics simulation of the mechanical behavior of sodium aluminosilicate geopolymer and calcium silicate hydrate composites. Comput. Mater. Sci. **150**, 500–509 (2018)
8. Hou, D., Ma, H., Zhu, Y., Li, Z.: Calcium silicate hydrate from dry to saturated state: structure, dynamics and mechanical properties. Acta Mater. **67**, 81–94 (2014)
9. Sarkar, P.K., Mitra, N.: Molecular level study of uni/multi-axial deformation response of tobermorite 11 Å: a force field comparison study. Cem. Concr. Res. **145**, 106451 (2021)
10. Kovačević, G., Nicoleau, L., Nonat, A., Veryazov, V.: Revised atomistic models of the crystal structure of C–S–H with high C/S ratio. Z. Phys. Chem. **230**, 1411–1424 (2016)
11. Hou, D., Zhang, J., Li, Z., Zhu, Y.: Uniaxial tension study of calcium silicate hydrate (C–S–H): structure, dynamics and mechanical properties. Mater. Struct. **48**, 3811–3824 (2014)
12. Hou, D., Li, H., Zhang, L., Zhang, J.: Nano-scale mechanical properties investigation of C–S–H from hydrated tri-calcium silicate by nano-indentation and molecular dynamics simulation. Constr. Build. Mater. **189**, 265–275 (2018)
13. Ayuela, A., Dolado, J.S., Campillo, I., de Miguel, Y.R., Erkizia, E., Sanchez-Portal, D., Rubio, A., Porro, A., Echenique, P.M.: Silicate chain formation in the nanostructure of cement-based materials. J. Chem. Phys. **127**, 164710 (2007)
14. Cong, X., Kirkpatrick, R.J.: ^{29}Si MAS NMR study of the structure of calcium silicate hydrate. Adv. Cem. Based Mater. **3**, 144–156 (1996)
15. Pellenq, R.J.-M., Kushima, A., Shahsavari, R., Van Vliet, K.J., Buehler, M.J., Yip, S., Ulm, F.-J.: A realistic molecular model of cement hydrates. Proc. Natl. Acad. Sci. U.S.A. **106**, 16102–16107 (2009)
16. Chiang, Y., Chang, S.-W.: Bridging the gap between NMR measured mean silicate chain length and nano-scale silicate polymorphism of calcium silicate hydrates. Cem. Concr. Res. **140**, 106268 (2021)
17. Allen, A.J., Thomas, J.J., Jennings, H.M.: Composition and density of nanoscale calcium-silicate-hydrate in cement. Nature Mater. **6**, 311–316

18. Cygan, R.T., Liang, J.-J., Kalinichev, A.G.: Molecular models of hydroxide, oxyhydroxide, and clay phases and the development of a general force field. J. Phys. Chem. B **108**, 1255–1266 (2004)
19. Shahsavari, R., Pellenq, R.J., Ulm, F.J.: Empirical force fields for complex hydrated calcio-silicate layered materials. Phys. Chem. Chem. Phys. **13**, 1002–1011 (2011)
20. Manzano, H., Pellenq, R.J., Ulm, F.J., Buehler, M.J., van Duin, A.C.: Hydration of calcium oxide surface predicted by reactive force field molecular dynamics. Langmuir **28**, 4187–4197 (2012)
21. Hou, D., Zhao, T., Ma, H., Li, Z.: Reactive molecular simulation on water confined in the nanopores of the calcium silicate hydrate gel: structure, reactivity, and mechanical properties. J. Phys. Chem. C **119**, 1346–1358 (2015)
22. Zhou, J., Liang, Y.: Effect of water on the dynamic tensile mechanical properties of calcium silicate hydrate: based on molecular dynamics simulation. Materials **12**, 2837 (2019)
23. Tao, L., Shahsavari, R.: Diffusive, displacive deformations and local phase transformation govern the mechanics of layered crystals: the case study of tobermorite. Sci. Rep. **7**, 5907 (2017)
24. Jennings, H.M.: Refinements to colloid model of C–S–H in cement: CM-II. Cem. Concr. Res. **38**, 275–289 (2008)
25. Bernal, J.D., Fowler, R.H.: A theory of water and ionic solution, with particular reference to hydrogen and hydroxyl ions. J. Chem. Phys. **1**, 515–548 (1933)
26. Guillot, B.: A reappraisal of what we have learnt during three decades of computer simulations on water. J. Mol. Liq. **101**, 219–260 (2002)
27. Chen, J.J., Thomas, J.J., Taylor, H.F.W., Jennings, H.M.: Solubility and structure of calcium silicate hydrate. Cem. Concr. Res. **34**, 1499–1519 (2004)
28. Abdolhosseini Qomi, M.J., Krakowiak, K.J., Bauchy, M., Stewart, K.L., Shahsavari, R., Jagannathan, D., Brommer, D.B., Baronnet, A., Buehler, M.J., Yip, S., Ulm, F.J., Van Vliet, K.J., Pellenq, R.J.-M.: Combinatorial molecular optimization of cement hydrates. Nature Commun. **5**, 4960 (2014)
29. Thompson, A.P., Aktulga, H.M., Berger R., Bolintineanu, D.S., Brown, W.M., Crozier, P.S., in't Veld, P.J., Kohlmeyer, A., Moore, S.G., Nguyen, T.D., Shan, R., Stevens, M.J., Tranchida, J., Trott, C., Plimpton, S.J.: LAMMPS—a flexible simulation tool for particle-based materials modeling at the atomic, meso, and continuum scales. Comput. Phys. Commun. **271**, 108171 (2022)
30. Constantinides, G., Ulm, F.-J.: The nanogranular nature of C–S–H. J. Mech. Phys. Solids **55**, 64–90 (2007)
31. Ulm, F.-J., Vandamme, M., Bobko, C., Alberto, O.J., Tai, K., Ortiz, C.: Statistical indentation techniques for hydrated nanocomposites: concrete, bone, and shale. J. Am. Ceram. Soc. **90**, 2677–2692 (2007)
32. Hill, R.: The elastic behaviour of a crystalline aggregate. Proc. Phys. Soc. Sect. A **65**, 349–354 (1952)
33. Voigt, W.: Lehrbuch der Kristallphysik. Taubner, Leipzig (1928)
34. Reuss, A.: Berechnung der fließgrenze von mischkristallen auf grund der plastizitätsbedingung für einkristalle. ZAMM J. Appl. Math. Mech./Z. Angew. Math. Mech. **9**, 49–58 (1929)
35. Constantinides, G., Ulm, F.-J.: The effect of two types of C–S–H on the elasticity of cement-based materials: results from nanoindentation and micromechanical modeling. Cem. Concr. Res. **34**, 67–80 (2004)
36. Hu, C., Han, Y., Gao, Y., Zhang, Y., Li, Z.: Property investigation of calcium-silicate-hydrate (C–S–H) gel in cementitious composites. Mater. Charact. **95**, 129–139 (2014)
37. Acker, P.: Swelling, shrinkage and creep: a mechanical approach to cement hydration. Mater. Struct. **37**, 237–243 (2004)
38. Hou, D., Zhu, Y., Lu, Y., Li, Z.: Mechanical properties of calcium silicate hydrate (C–S–H) at nano-scale: a molecular dynamics study. Mater. Chem. Phys. **146**, 503–511 (2014)
39. Hou, D., Zhao, T., Wang, P., Li, Z., Zhang, J.: Molecular dynamics study on the mode I fracture of calcium silicate hydrate under tensile loading. Eng. Fract. Mech. **131**, 557–569 (2014)

40. Shahsavari, R., Buehler, M.J., Pellenq, R.J.M., Ulm, F.-J.: First-principles study of elastic constants and interlayer interactions of complex hydrated oxides: case study of tobermorite and Jennite. J. Am. Ceram. Soc. **92**, 2323–2330 (2009)
41. Manzano, M.H.: Atomistic simulation studies of the cement paste components. Servicio Editorial de la Universidad del País Vasco/Euskal Herriko Unibertsitatearen Argitalpen Zerbitzua (2009)
42. Tongraar, A., Liedl, K.R., Rode, B.M.: Solvation of Ca^{2+} in water studied by born-oppenheimer ab Initio QM/MM dynamics. J. Phys. Chem. A **101**, 6299–6309 (1997)
43. Soyer-Uzun, S., Chae, S.R., Benmore, C.J., Wenk, H.-R., Monteiro, P.J.M., Brown, P.: Compositional evolution of calcium silicate hydrate (C–S–H) structures by total X-ray scattering. J. Am. Ceram. Soc. **95**, 793–798 (2012)
44. Merlino, S., Bonaccorsi, E., Armbruster, T.: Tobermorites: their real structure and order-disorder (OD) character. Am. Miner. **84**, 1613–1621 (1999)
45. Xin, H., Lin, W., Fu, J., Li, W., Wang, Z.: Temperature effects on tensile and compressive mechanical behaviors of C–S–H structure via atomic simulation. J. Nanomater. **2017**, 1–6 (2017)
46. Manzano, H., Moeini, S., Marinelli, F., van Duin, A.C., Ulm, F.J., Pellenq, R.J.: Confined water dissociation in microporous defective silicates: mechanism, dipole distribution, and impact on substrate properties. J. Am. Chem. Soc. **134**, 2208–2215 (2012)
47. Teleman, O., Jönsson, B., Engström, S.: A molecular dynamics simulation of a water model with intramolecular degrees of freedom. Mol. Phys. **60**, 193–203 (1987)
48. Ho, T.A., Striolo, A.: Molecular dynamics simulation of the graphene-water interface: comparing water models. Mol. Simul. **40**, 1190–1200 (2014)
49. Jorgensen, W.L., Chandrasekhar, J., Madura, J.D., Impey, R.W., Klein, M.L.: Comparison of simple potential functions for simulating liquid water. J. Chem. Phys. **79**, 926–935 (1983)
50. Jorgensen, W.L., Madura, J.D.: Temperature and size dependence for Monte Carlo simulations of TIP4P water. Mol. Phys. **56**, 1381–1392 (2006)
51. Røn, T., Lee, S.: Influence of temperature on the frictional properties of water-lubricated surfaces. Lubricants **2**, 177–192 (2014)
52. Briscoe, W.H.: Aqueous boundary lubrication: molecular mechanisms, design strategy, and terra incognita. Curr. Opin. Colloid Interface Sci. **27**, 1–8 (2017)
53. Ewen, J., Heyes, D., Dini, D.: Advances in nonequilibrium molecular dynamics simulations of lubricants and additives. Friction **6**, 349–386 (2018)
54. Wang, X., Gong, L.-X., Tang, L.-C., Peng, K., Pei, Y.-B., Zhao, L., Wu, L.-B., Jiang, J.-X.: Temperature dependence of creep and recovery behaviors of polymer composites filled with chemically reduced graphene oxide. Compos. Part A Appl. Sci. Manuf. **69**, 288–298 (2015)
55. Anand, A., Banerjee, P., Sahoo, D., Rathore, D.K., Prusty, R.K., Ray, B.C.: Effects of temperature and load on the creep performance of CNT reinforced laminated glass fiber/epoxy composites. Int. J. Mech. Sci. **150**, 539–547 (2019)
56. Jian, W., Lau, D.: Creep performance of CNT-based nanocomposites: a parametric study. Carbon **153**, 745–756 (2019)
57. Qiu, M., Miao, Y., Li, Y., Lu, J.: Influence of ultrasonic modified liners on the adhesive and tribological performances of self-lubricating radial spherical plain bearings. Tribol. Trans. **59**, 655–662 (2016)
58. Feng, D., Li, X., Wang, X., Li, J., Zhang, X.: Capillary filling under nanoconfinement: the relationship between effective viscosity and water-wall interactions. Int. J. Heat Mass Transf. **118**, 900–910 (2018)
59. Kai, M.F., Zhang, L.W., Liew, K.M.: Carbon nanotube-geopolymer nanocomposites: a molecular dynamics study of the influence of interfacial chemical bonding upon the structural and mechanical properties. Carbon **161**, 772–783 (2020)
60. Bair, S., Jarzynski, J., Winer, W.O.: The temperature, pressure and time dependence of lubricant viscosity. Tribol. Int. **34**, 461–468 (2001)

61. Kai, M.F., Zhang, L.W., Liew, K.M.: Graphene and graphene oxide in calcium silicate hydrates: chemical reactions, mechanical behavior and interfacial sliding. Carbon **146**, 181–193 (2019)
62. Zhou, Y., Zheng, H., Li, W., Ma, T., Miao, C.: A deep learning potential applied in tobermorite phases and extended to calcium silicate hydrates. Cem. Concr. Res. **152**, 106685 (2022)